Evaluating the Effect of Tissue Anisotropy on Brain Tumor Growth Using a Mechanically Coupled Reaction–Diffusion Model

Daniel Abler, Russell C. Rockne and Philippe Büchler

Abstract Glioblastoma (GBM) is the most frequent malignant brain tumor in adults and presents with different growth phenotypes. We use a mechanically coupled reaction–diffusion model to study the influence of structural brain tissue anisotropy on tumor growth. Tumors were seeded at multiple locations in a human MR-DTI brain atlas and their spatiotemporal evolution was simulated using the Finite Element Method. We evaluated the impact of tissue anisotropy on the model's ability to reproduce the aspherical shapes of real pathologies by comparing predicted lesions to publicly available GBM imaging data. The impact of tissue anisotropy on tumor shape was strongly location dependent and highest for tumors in brain regions with a single dominating white matter fiber direction, such as the corpus callosum. Despite strongly anisotropic growth assumptions, all simulated tumors remained more spherical than real lesions at the corresponding anatomic location and similar volume. These findings confirm previous simulation studies, suggesting that cell migration along WM fiber tracks is not a major determinant of tumor shape in the setting of reaction–diffusion-based tumor growth models and for most locations across the brain.

Keywords Glioma · Anisotropy · DTI · Mass effect · Reaction–diffusion model · Biomechanics

D. Abler (✉) · P. Büchler
ARTORG Center for Biomedical Engineering Research, University of Bern, Bern, Switzerland
e-mail: daniel.abler@artorg.unibe.ch

P. Büchler
e-mail: philippe.buechler@artorg.unibe.ch

D. Abler · R. C. Rockne
Beckman Research Institute, City of Hope, Duarte, CA, USA
e-mail: rrockne@coh.org

J. M. R. S. Tavares and P. R. Fernandes (eds.), *New Developments on Computational Methods and Imaging in Biomechanics and Biomedical Engineering*, Lecture Notes in Computational Vision and Biomechanics 33, https://doi.org/10.1007/978-3-030-23073-9_3

1 Introduction

Gliomas are the most frequent primary brain tumors in adults (70%) [15]. Glioblastoma Multiforme (GBM) is the most malignant subtype of glioma, accounting for about 50% of diffuse gliomas. GBM infiltrates surrounding healthy tissue, grows rapidly, and forms a necrotic core of high cell density which is frequently accompanied by compression and displacement of the surrounding tissue. Despite aggressive treatment, long-term prognosis remains poor with median overall survival below 1.5 years [15].

Invasive growth and mass-effect are the macroscopic hallmarks of GBM. Variability can be observed with regard to these characteristics, ranging from predominantly invasive tumors without notable mass-effect to strongly displacing ones that induce higher mechanical stresses and result in healthy tissue deformation, midline shift, or herniation. These solid stresses play an important role for tumor evolution [9], which suggests that biomechanical factors have direct implications not only on the biophysical level, but may affect treatment response and outcome.

We have previously developed a mechanically coupled reaction–diffusion model of brain tumor growth that accounts for tumor mass-effect [1]. This framework simulates tumor evolution over time and across different brain regions using literature-based parameter estimates for tumor cell proliferation, as well as isotropic motility, and mechanical tissue properties. The model yielded realistic estimates of the mechanical impact of a growing tumor on intracranial pressure, however, comparison to imaging data showed that asymmetric shapes could not be reproduced.

To investigate the role of tissue anisotropy on simulated tumor shape, we extended our simulation framework to take into account tissue structure. White matter consists predominantly of aligned axonal fibers, whose orientation can be inferred from Magnetic Resonance (MR) Diffusion Tensor Imaging (DTI), which measures water diffusion along different directions in space. As diffusion is constrained transverse to fiber direction, MR-DTI provides structural information of brain tissue. Information from MR-DTI has previously been used to inform tumor cell migration behavior in mathematical models of brain tumor growth, see [17, table 1] for an overview of related work.

The few studies that have investigated the effect of tissue anisotropy on larger patient cohorts found it to have a beneficial, but relatively small effect on their models' ability to reproduce real tumor shapes. Employing the anisotropic glioma spread model of [14], [17] investigated the effect of tissue anisotropy without mass-effect. Their study on 10 cases showed an improved ability to approximate tumor shapes (average increase in Jaccard score by 0.03 ± 0.03, about 5% relative to the isotropic case) when including patient-specific DTI information and personalized estimates for a patient-specific anisotropy parameter that describes the sensitivity of cancer cells to the underlying brain structure. Only a few studies [3, 5, 6] took into account the tumor's mass effect when investigating the effect of tissue anisotropy. Simulation results of 9 low-grade glioma cases were reported by [6], using patient-specific DTI information, non-personalized growth parameters and an isotropic viscoelastic

material model for brain tissue. Using DTI information in their study improved the Jaccard Score (Dice Index) between simulated and actual tumor by $\leq$2.40% ($\leq$1.50%).

In the present study, we investigate the combined effect of anisotropic growth and mechanical tissue characteristics on tumor shape in a mechanically coupled reaction–diffusion model of invasive glioma growth by comparing simulation results obtained from isotropic and anisotropic material assumptions.

2 Materials and Methods

Figure 1 illustrates the study setup: Virtual tumors were seeded in an atlas of healthy brain anatomy at representative locations extracted from 10 subjects of the BRATS 2013[1] [11, 12] training dataset. Figure 2 shows the spatial distribution of the selected lesions in a human brain atlas. Tumor growth evolution was simulated for isotropic and anisotropic tissue properties and two sets of growth parameter choices, corresponding to diffuse and nodular growth characteristics, respectively. Virtually grown and real tumors were compared when the simulated tumor had reached the tumor volume of the corresponding subject from the BRATS dataset.

2.1 Mathematical Model

The mathematical model used in this study captures three interrelated aspects of macroscopic glioma growth [1]: Cell proliferation, invasion of tumor cells into the surrounding healthy tissue, and tissue deformation due to the tumor-induced mass-effect.

We model the invasive growth of glioma phenomenologically as a Reaction–Diffusion (RD) process [19], representing cell migration by passive diffusion:

$$\frac{\partial q}{\partial t} = \nabla \cdot \left(\hat{\mathsf{D}} \, \nabla q \right) + \rho \, q \, (1 - q) \ , \tag{1}$$

with normalized cancer cell concentration $q(\mathbf{r}, t)$ and diffusion tensor $\hat{\mathsf{D}} = \hat{\mathsf{D}}(\mathbf{r})$. Tumor growth is modeled as a logistic growth process with proliferation rate ρ.

Similarly to [3, 5], the tissue-displacing mass-effect of the growing tumor is represented phenomenologically using a linear-elastic solid mechanics approach. It relies on the assumption that the creation of new tumor cells leads to volumetric

[1] https://www.smir.ch/BRATS/Start2013.

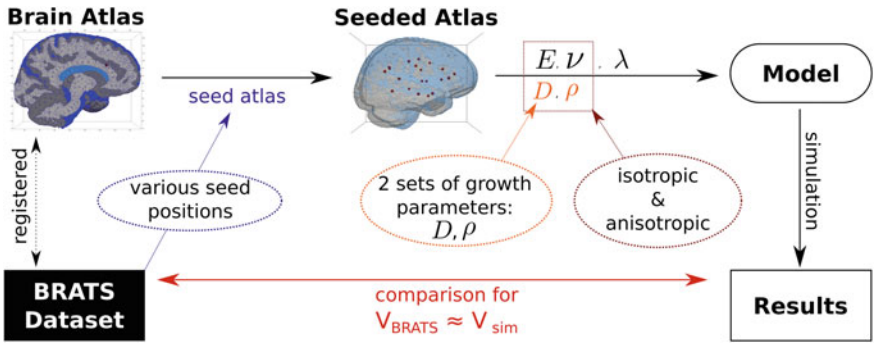

Fig. 1 Tumor growth evolution was simulated in a healthy brain atlas for two sets of growth parameters (D, ρ), and isotropic and anisotropic tissue properties. Simulated tumors were compared to subjects from the BRATS data set at approximately identical volume

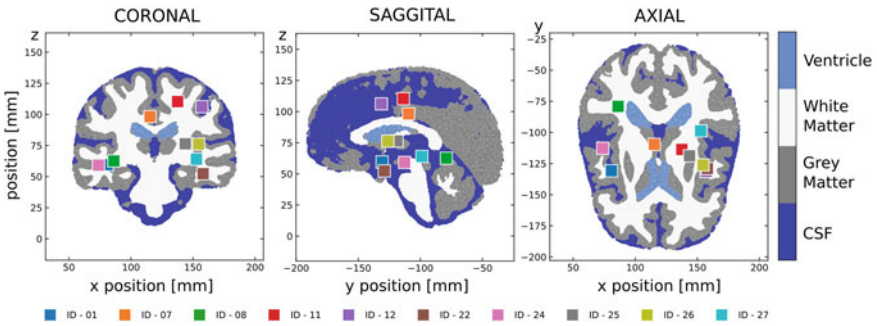

Fig. 2 Tumor center-of-mass positions of 10 selected BRATS cases projected onto central planes of SRI24 atlas

increase of the tumor and thus results in an expansion of the affected brain tissue. The volumetric increase is modeled by introducing a growth-induced strain component $\hat{\varepsilon}^{\text{growth}}(q)$, so that

$$\hat{\varepsilon}^{\text{total}}(\mathbf{u}, q) = \hat{\varepsilon}^{\text{elastic}}(\mathbf{u}) + \hat{\varepsilon}^{\text{growth}}(q) \ . \tag{2}$$

where displacements $\mathbf{u}$ are obtained from solving the linear-momentum equilibrium equation with stress $\hat{\sigma}(\mathbf{u})$ and strain $\hat{\varepsilon}^{\text{total}}(\mathbf{u})$ linked by a linear constitutive relationship.

Additionally, we assume a linear coupling between tumor cell concentration and growth-induced strain

$$\hat{\varepsilon}^{\text{growth}}(q) = \hat{\lambda}\, q = \lambda\, \mathbb{1}\, q \ , \tag{3}$$

with isotropic coupling strength λ.

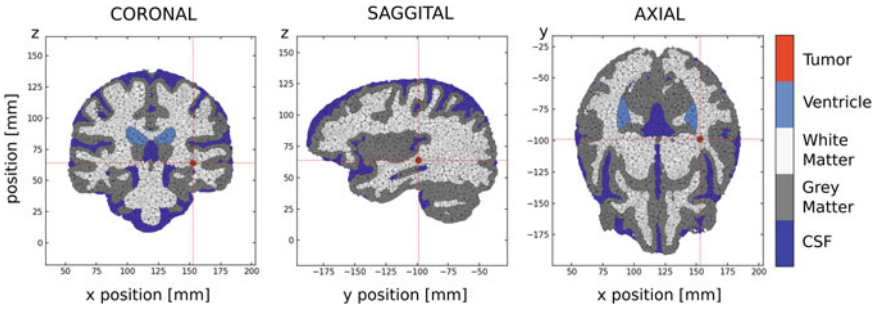

Fig. 3 Projections through seeded SRI24 atlas. An exemplary seed location is shown in the tetrahedral mesh used for simulation

2.2 Simulation Domain

We used the SRI24[2] [16] atlas of normal human brain anatomy to define the simulation geometry with tissue classes. Release 2.0 of the atlas provides separate tissue labels for White Matter (WM), Grey Matter (GM), and Cerebrospinal Fluid (CSF). We divided the CSF domain into two compartments to distinguish fluid-filled brain ventricles from the remaining CSF, surrounding the brain tissue. Additionally, the map of dominant Diffusion Tensor Imaging (DTI) eigenvectors was obtained from an earlier release (v0.0) of the atlas. This information was interpreted as local orientation of axon fibers and was used to inform diffusion and mechanical tissue parameters in the anisotropic simulation scenario. Finally, all relevant components of the atlas were registered to fit the spatial orientation of the BRATS datasets.

The tumor center-of-mass position was computed for each of the 10 selected subjects, based on the tumor volume visible on T1-weighted contrast-enhanced (T1c) MR imaging. For each subject, a spherical tumor seed (2 mm radius) was introduced in the atlas label map at the corresponding center-of-mass position, and a tetrahedral mesh was generated (approximately 320 000 elements) using CGAL[3] and VTK[4] libraries. DTI information from the SRI24 atlas was then interpolated over the seeded mesh. Figure 3 shows coronal, sagittal, and axial views through an exemplary seeded and meshed simulation domain.

[2] https://www.nitrc.org/projects/sri24/.

[3] https://www.cgal.org.

[4] https://www.vtk.org.

2.3 Simulation Assumptions

To compare the effect of tissue anisotropy on the evolution of tumor characteristics, two different simulation scenarios were considered, assuming isotropic and anisotropic material properties, respectively.

In both cases, the brain tissues WM and GM were modeled as linear-elastic materials. The CSF of the brain ventricles was modeled as compressible to account for physiological mechanisms that compensate elevated intracranial pressure [21], whereas the remaining CSF was modeled as nearly incompressible. Simulations were run with two distinct sets of growth parameters corresponding to *nodular* and *diffuse* growth characteristics with $\rho/D \geq 1.35\,\mathrm{mm}^{-2}$ and $\rho/D \leq 0.37\,\mathrm{mm}^{-2}$ [2], respectively. A maximum tumor-induced strain of 15% [13] was assumed, $\lambda = 0.15$, and an initial condition of $q = 1$ over the entire volume of the tumor seed was imposed. Deformation of the brain surface and escape of tumor cells from the brain were constrained by zero-displacement and zero-flux boundary conditions at surface nodes. The mathematical model was solved using the Finite Element Method. It was implemented in Abaqus (Simulia, Dassault Systémes) as fully coupled thermal stress analysis using 4-node linear elements (C3D4T) with the tumor mass-effect being represented by volumetric thermal expansion.

Isotropic Scenario

In the isotropic simulation scenario, diffusion and mechanical tissue behavior were assumed isotropic using the parameter values summarized in Tables 1 and 2 for the considered tissue types. The linear material model was fully characterized by two

Table 1 Reaction–diffusion parameter sets (D, ρ), representing *nodular* and *diffuse growth*. Tissue-specific motility estimates (D_{WM}, D_{GM}) are based on the assumption that D_{avg} was measured in a tissue volume containing equal portions of GM and WM, and $D_{\mathrm{WM}} = 5D_{\mathrm{GM}}$ [19]

Growth type	ρ [1/d]	D_{avg} [mm^2/d]	D_{avg}/ρ [mm^2]	ρ/D_{avg} [mm^{-2}]	D_{GM} [mm^2/d]	D_{WM} [mm^2/d]
Nodular	0.082	0.053	0.650	1.540	0.020	0.101
Diffuse	0.037	0.105	2.855	0.350	0.040	0.200

Table 2 Mechanical tissue properties (isotropic case), informed by [21]

Tissue	E [kPa]	ν
W/G Matter	3.0	0.45
Tumor	6.0	0.45
CSF (Ventricles)	1.0	0.30
CSF (other)	1.0	0.49

parameters, Poisson ratio ν and Young's modulus E. Values for Young's modulus of brain tissue and tumor were adopted from [21].

Anisotropic Scenario

In the anisotropic simulation scenario, white matter fiber directionality was taken into account and the tissue was modeled as transversely isotropic material with different material properties along ($\parallel$) and orthogonal to ($\perp$) the fibers.

Tumor cell motility along fiber direction (WM) was assumed identical to the isotropic case $D_{\mathrm{W}}^{\parallel} = D_{\mathrm{W}}^{\mathrm{iso}}$, whereas a significantly lower motility was chosen for the transverse direction $D_{\mathrm{W}}^{\perp} = 0.01 D_{\mathrm{W}}^{\mathrm{iso}}$. Due to reduced fiber alignment, cell motility in grey matter was modeled as isotropic [3, 5] with the value indicated in Table 1. We chose a very high ratio $D_{\mathrm{W}}^{\parallel}/D_{\mathrm{W}}^{\perp} = 100$ to investigate the effect of growth anisotropy. For comparison, [6] assumed a ratio of 5; [10] varied this ratio between 5 and 100 and found the best "de visu" fit for a ratio of 10.

Linear-elastic mechanical tissue properties of the transversely isotropic situation can be expressed in terms of seven engineering constants: Two Young's moduli that describe the stresses resulting from uniaxial stretch parallel $E^{\parallel}$ and perpendicular $E^{\perp}$ to the fiber axis. Two shear moduli that describe shear stresses in planes parallel to ($\mu^{\parallel}$) and normal to ($\mu^{\perp}$) the fiber axis. Three Poisson ratios $\nu^{\parallel\perp}$, $\nu^{\perp\parallel}$, $\nu^{\perp\perp}$ that describe the strain in one direction ($\parallel$ or $\perp$) that arises from stretch in another orthogonal direction ($\parallel$ or $\perp$). Only five of these seven parameters are typically independent since additionally:

$$\frac{\nu^{\parallel\perp}}{E^{\parallel}} = \frac{\nu^{\perp\parallel}}{E^{\perp}} \tag{4a}$$

$$\mu^{\perp} = \frac{E^{\perp}}{2(1+\nu^{\perp\perp})}\,. \tag{4b}$$

To estimate parameters of that model, we assume a fiber reinforcement effect in white matter that increases resistance against stretch along the fiber direction, $E_W^{\parallel} = 3 \cdot E_W^{\perp}$, from observations on lamb corpus callosum $E^{\parallel}/E^{\perp} \approx 6.5$ [7] and porcine corona radiata $E^{\parallel}/E^{\perp} \approx 2.7$ [7, 20]. Based on the material parameters used for the isotropic cases, we defined the Young's moduli of white matter so that $E_{\mathrm{WM}}^{\parallel} > E_{\mathrm{GM}}^{\mathrm{iso}} > E_{\mathrm{WM}}^{\perp}$. We assume $\nu^{\parallel\perp} = \nu^{\mathrm{iso}}$, so that $\nu^{\perp\parallel}$ follows from Eq. (4a) and $\nu^{\perp\perp} = 1 - \nu^{\perp\parallel}$. This allows us to compute $\mu^{\perp}$ from Eq. (4b). We then compute $\mu^{\parallel} = 1.4\,\mu^{\perp}$ [7]. Resulting mechanical model parameters for white matter are summarized in Table 3.

2.4 Analysis

Two different tumor detection thresholds were used to evaluate simulation results: $c_{\mathrm{T1c}} = 0.80$ and $c_{\mathrm{T2}} = 0.16$ corresponding to tumor features visible on T1-weighted

contrast enhanced (T1c) and T2-weighted (T2) MRI imaging [18], respectively. Simulations were run until the simulated tumor had reached the T1c volume of the corresponding BRATS subject. Tumors corresponding to T1c and T2 visibility threshold were extracted at multiples of 5mm increments in equivalent radius computed from the simulated T1c volume. For each tumor volume, the following measures were computed: (a) Tumor *aspect ratio*, as the ratio between the shortest and longest axis of the smallest bounding box around the tumor. A value of 1 corresponds to a spherical tumor shape; values closer to 0 indicate aspherical (elongated, oblate, or asymmetric) shapes. (b) Tumor *nodularity*, as the ratio of T1c and T2 tumor volumes. A value close to 1 corresponds to a very well delineated, nodal tumor, whereas values closer to 0 indicate diffuse growth.

The same measures were computed from BRATS segmentations by identifying the T1c tumor volume with labels {necrotic, non-enhancing tumor, enhancing tumor} and the T2 volume with labels {necrotic, non-enhancing tumor, enhancing tumor, edema}. Measures derived from simulated tumors and real pathologies were compared at similar volumes $V_{\text{T1c, sim}} \approx V_{\text{T1, BRATS}}$.

3 Results

Tumor growth evolution and tissue deformation were simulated for all 10 selected BRATS subjects, growth parameterizations (nodular, diffuse) and tissue structure scenarios (isotropic, anisotropic).

The anisotropic growth scenario showed an average 4.3 ± 6.2 % reduction of tumor aspect ratio compared to isotropic growth assumptions. The impact on tumor shape was similar for *diffuse* ($3.9 \pm 7.6\%$) and *nodular* ($4.7 \pm 4.6\%$) growth parameterizations. However, both isotropic and anisotropic growth assumptions resulted in simulated tumor shapes that were more spherical than the corresponding BRATS lesions, Fig. 4.

The effect of tissue anisotropy on simulated tumor shape was strongly dependent on seed location: Tumors grown from seeds located deep in WM (ID-07, ID-27) and adjacent to the lateral ventricle (ID-08) exhibited a strong effect of tissue anisotropy.

Table 3 Mechanical tissue properties (anisotropic simulation scenario), assuming transverse symmetry with directions along ($\parallel$) and orthogonal to ($\perp$) fiber direction. Material properties for GM and CSF were those from Table 2

Tissue	$E^{\parallel}$ [kPa]	$E^{\perp}$ [kPa]	$\mu^{\parallel}$ [kPa]	$\mu^{\perp}$ [kPa]	$\nu^{\parallel\perp}$	$\nu^{\perp\parallel}$	$\nu^{\perp\perp}$
White matter	4.5	1.5	0.56	0.40	0.45	0.15	0.85
Tumor (if in WM)	9.0	3.0	1.12	0.8	0.45	0.15	0.85

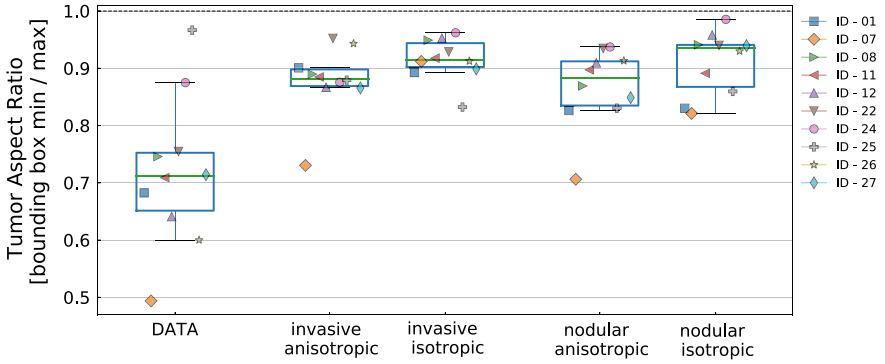

Fig. 4 Aspect ratio of BRATS T1c lesions and simulated tumors for diffuse/nodular growth parameterization and isotropic/anisotropic tissue properties. A value of 1 indicates a spherical shape, whereas lower values correspond to oblate or elongated shapes

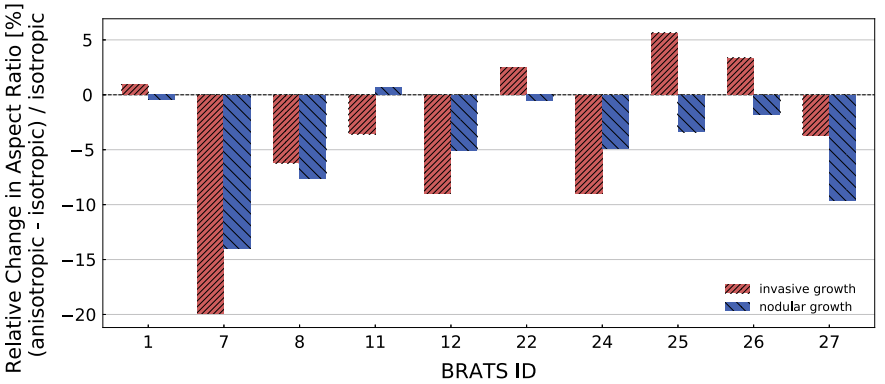

Fig. 5 Relative change in tumor aspect ratio between isotropic and anisotropic configurations. A negative value corresponds to a decrease in aspect ratio due to anisotropic material properties

Seeds located closer to WM/GM interfaces (ID-11, ID-12, ID-22, ID-24) showed mixed effects, while those located in GM (ID-01, ID-25, ID-26) experienced only small effects, Fig. 5. These observations are consistent with our parameterization which considers GM to be isotropic. The effect of tissue anisotropy on shape was particularly pronounced for ID-07 located medially in the corpus callosum, a region of highly aligned axons.

Tumor nodularity extracted from BRATS images (*DATA* in Fig. 6) differed across the selected cases. For each simulated BRATS case, the computed nodularity measure was consistent with growth parameterization: lower for diffuse and higher for nodal growth. In most cases, the anisotropic growth scenario resulted in more nodular tumors compared to isotropic growth assumptions, due to reduced overall diffusivity. Despite identical growth parameterization (nodular, diffuse), the computed nodularity of simulated tumors differed across BRATS subjects. This effect can be

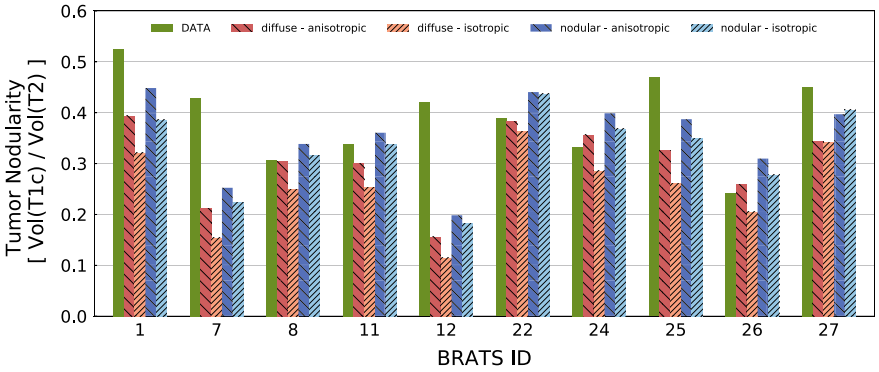

Fig. 6 Tumor nodularity of BRATS lesions and simulated tumors for diffuse/nodular growth parameterization and isotropic/anisotropic tissue properties. A value close to 1 corresponds to a nodular tumor, whereas smaller values indicate diffuse growth

attributed to differences in the growth environment (WM, GM, boundary, constrained by CSF/ventricle) resulting in distinct average growth parameters for each lesion.

4 Discussion

This study explored the effect of tissue anisotropy on glioma growth simulations in a 3D human brain atlas. In agreement with model parameterization, we found tissue anisotropy to result in reduced tumor shape symmetry for tumors located in WM and for some lesions at the WM/GM interface. However, despite choosing strongly anisotropic diffusion parameters, $D_{\mathrm{W}}^{\parallel}/D_{\mathrm{W}}^{\perp} = 100$, all simulated tumors remained more spherical than real lesions at the corresponding anatomical location and of similar volume.

Our findings confirm findings of previous simulation studies [6, 17] suggesting that anisotropic cell migration along WM fiber tracks is not a major determinant of tumor shape in the setting of reaction–diffusion-based tumor growth models and for most locations across the brain. Exceptions might apply for tumors located in brain regions where a single dominant fiber direction prevails throughout a larger contiguous volume segment. For example, in this study, we observed the highest relative change in aspect ratio due to tissue anisotropy, 14–20%, for a medially located GBM in the corpus callosum (ID-07).

Large variability in tumor nodularity for identical growth parameterizations (diffuse/nodular) across different brain locations, Fig. 6, indicates that 3D tumor growth is strongly affected by the tissue composition of a tumor's growth domain. We hypothesize that the interplay between tissue composition, spatial constraints, and resulting mechanical forces may exceed the effect of tissue anisotropy on tumor growth, possibly giving rise to location-specific growth archetypes of GBM.

While our model computed tumor mass-effect and resulting in healthy tissue deformation, neither this nor similar previous modeling studies for human GBM [6, 17] captured the growth-inhibiting effect of solid stress [8].

The present study has further limitations: (a) Only the tumor seed position was personalized for each growth model, not the brain anatomy or growth parameters. A mismatch between patient and atlas anatomy and/or asymmetric growth may have resulted in the simulated tumor growth process being initialized in a different brain tissue, which can significantly affect the tumor's simulated evolution. This may explain shape discrepancies for some of the BRATS cases, such as ID-25 (ID-26) which has a very high (low) aspect ratio in the BRATS dataset, but ranges among the simulated tumor shapes with lowest (highest) aspect ratio. (b) DTI information was derived from an atlas of the healthy human brain so that possible changes in local tissue structure due to tumor growth could not be taken into account. We considered brain tissues to be either isotropic (GM) or anisotropic (WM), not distinguishing varying degrees of anisotropy within each tissue class. Also, possible differences in patient-specific sensitivity of cancer cells to the underlying brain structure were not taken into account. (c) This study relied on a linear-elastic material model with estimates for mechanical tissue anisotropy derived from animal brain tissue characterization. Recent evidence [4] suggests that an Ogden material model captures the mechanical response of human brain tissue more accurately.

5 Conclusion

This study investigated the joint impact of tumor mass effect and tissue anisotropy on simulated tumor shape. In agreement with previous simulation studies, we find that anisotropic cell migration along WM fiber tracks is not a major determinant of tumor shape, except for growth locations where a single dominant fiber direction prevails throughout a larger contiguous volume segment. Further work is needed to combine the individual contributions of structural anisotropy, tissue composition, and mechanical growth constraints in a way to best reproduce GBM growth characteristics.

Acknowledgements The research leading to these results has received funding from the European Union's Horizon 2020 research and innovation programme under the Marie Skodowska-Curie grant agreement No 753878. Calculations were performed on UBELIX (http://www.id.unibe.ch/hpc), the HPC cluster at the University of Bern.

References

1. Abler D et al (2018) Evaluation of a mechanically coupled reaction-diffusion model for macroscopic brain tumor growth. In: Gefen A et al (eds) Computer methods in biomechanics and biomedical engineering. Springer International Publishing, Cham, pp 57–64

2. Baldock AL et al (2014) Patient-specific metrics of invasiveness reveal significant prognostic benefit of resection in a predictable subset of gliomas. LoS ONE 9(10):e99057
3. Bondiau P-Y et al (2008) Biocomputing: numerical simulation of glioblastoma growth using diffusion tensor imaging. Phys Med Biol 53(4):879–893
4. Budday S et al (2017) Mechanical characterization of human brain tissue. Acta Biomater 48:319-340
5. Clatz O et al (2005) Realistic simulation of the 3-D growth of brain tumors in MR images coupling diffusion with biomechanical deformation. IEEE Trans Med Imaging 24(10):1334–1346
6. Elazab A et al (2017) Post-surgery glioma growth modeling from magnetic resonance images for patients with treatment. Sci Rep 7(1)
7. Feng Y et al (2013) Measurements of mechanical anisotropy in brain tissue and implications for transversely isotropic material models of white matter. J Mech Behav Biomed Mater 23:117–132
8. Helmlinger G et al (1997) Solid stress inhibits the growth of multicellular tumor spheroids. Nat Biotechnol 15(8):778–783
9. Jain RK et al (2014) The role of mechanical forces in tumor growth and therapy. Annu Rev Biomed Eng 16(1):321–346
10. Jbabdi S et al (2005) Simulation of anisotropic growth of low-grade gliomas using diffusion tensor imaging. Magn Reson Med 54(3):616–624
11. Kistler M et al (2013) The virtual skeleton database: an open access repository for biomedical research and collaboration. J Med Internet Res 15(11):e245
12. Menze B et al (2014) The multimodal brain tumor image segmentation benchmark (BRATS). IEEE Trans Med Imaging, p 33
13. Mohamed A et al (2005) Finite element modeling of brain tumor mass-effect from 3D medical images. In: Medical image computing and computer-assisted intervention-MICCAI 2005. Lecture notes in computer science 3749. Springer, Berlin, pp 400–408
14. Painter K et al (2013) Mathematical modelling of glioma growth: the use of diffusion tensor imaging (DTI) data to predict the anisotropic pathways of cancer invasion. J Theor Biol 323:25–39
15. Ricard D et al (2012) Primary brain tumours in adults. Lancet 379(9830):1984–1996
16. Rohlfing T et al (2009) The SRI24 multichannel atlas of normal adult human brain structure. Hum Brain Mapp 31(5):798–819
17. Swan A et al (2017) A patient-specific anisotropic diffusion model for brain tumour spread. Bull Math Biol
18. Swanson KR et al (2008) A mathematical modelling tool for predicting survival of individual patients following resection of glioblastoma: a proof of principle. Br J Cancer 98(1):113–119
19. Swanson KR et al (2000) A quantitative model for differential motility of gliomas in grey and white matter. Cell Prolif 33(5):317–329
20. Velardi F et al (2006) Anisotropic constitutive equations and experimental tensile behavior of brain tissue. Biomech Model Mechanobiol 5(1):53–61
21. Wittek A et al (2010) Patient-specific non-linear finite element modelling for predicting soft organ deformation in real-time; application to non-rigid neuroimage registration. Prog Biophys Mol Biol. Special Issue on Biomechanical Modelling of Soft Tissue Motion 103(2–3):292–303